frontiers | Frontiers in Earth Science

ORIGINAL RESEARCH
published: 13 April 2022
doi: 10.3389/feart.2022.878782

Experimental Study on the Accumulation Characteristics and Mechanism of Landslide Debris Dam

Xiangping Xie, Xiaojun Wang, Shenzhou Zhao, Zhongli Li, Xuyang Qin and Shu Xu*

Department of Civil and Architectural Engineering, Anyang Institute of Technology, Anyang, China

According to physical model tests, we analyzed the accumulation characteristics of landslide dams formed under three different slope characteristics, namely, uniform slope, parallel slope, and intersecting slope and investigated the accumulation mechanisms of the debris dams. The relationship between slope types and accumulation characteristics was also explored using the tracer particle analysis method. The damming process and accumulation mechanism of the landslide dam were changed with slope conditions, which lead to the difference in the accumulation characteristics of the dam, especially in transverse cross-sectional shape and grain size distribution. The transverse cross-sectional shape of the landslide dams formed by different slope conditions can be divided into three categories: the flat pattern, unidirectional pattern, and undulating pattern. The characteristics of the slope body are closely related to those of the landslide dam with respect to debris distribution. The debris distributions in the longitudinal and transverse directions of the slope body are consistent with those in the longitudinal and sliding regions of the dam. A general inverse grading characteristic of debris gains occurs in the vertical direction of landslide dams. For the uniform and parallel slopes, obvious inverse grading distribution is induced by overall-starting initiation of the slope body and strong vertical infiltration of the fine sands during the movement. However, inverse grading distribution is generated by the effects of pushing–climbing and lateral infiltration that existed among particles caused by a layered-starting mode for the intersecting slope body. This study provides a basis for the prediction of landslide dam formation and backtracks the initial structure of the slope.

Keywords: landslide dam, slope characteristic, accumulation characteristic, sorting mechanism, dynamic process

Edited by:
Dongri Song,
Institute of Mountain Hazards and Environment (CAS), China

Reviewed by:
Qiming Zhong,
Nanjing Hydraulic Research Institute, China
Hongchao Zheng,
Tongji University, China
Shaojie Zhang,
Institute of Mountain Hazards and Environment (CAS), China

****Correspondence:***
Xiangping Xie
xxp_imde@163.com

Specialty section:
This article was submitted to Geohazards and Georisks, a section of the journal Frontiers in Earth Science

Received: *18 February 2022*
Accepted: *21 March 2022*
Published: *13 April 2022*

Citation:
Xie X, Wang X, Zhao S, Li Z, Qin X and Xu S (2022) Experimental Study on the Accumulation Characteristics and Mechanism of Landslide Debris Dam. Front. Earth Sci. 10:878782. doi: 10.3389/feart.2022.878782

INTRODUCTION

According to statistical data worldwide, landslide and debris flow are the main reasons for the formation of barrier dams (Costa and Schuster, 1988; Shi et al., 2014; Nian et al., 2018; Zheng et al., 2021). They can block both large rivers and little channels. Earthquakes often induce a large number of landslides that form large-scale river-blocking dams, such as Tangjiashan landslide dam, Yangjiagou landslide dam induced by the 2008 Wenchuan earthquake, and Hongshiyan landslide dam triggered by the 2014 Ludian earthquake (Hu et al., 2009; Fan et al., 2012; Zhou J.-w. et al., 2013; Zhang et al., 2015; Shi et al., 2017). Such river-blocking dams have poor stability and often fail in a short time after their formation, which poses great threat to the lives and properties of the surrounding areas and downstream people. The Tangjiashan dam collapsed 29 days after its

formation, forcing 200,000 people downstream to evacuate (Shi et al., 2015). The Baige dam on the Jinsha River collapsed within 3 days, affecting more than 500 km downstream, forcing 25,000 people to evacuate (Fan et al., 2019). Meanwhile, as reported by Fan et al. (2012), the 2008 Wenchuan earthquake triggered approximately 60,000 co-seismic landslides, where only 800 or so blocked the rivers, and numerous more might form small and medium-sized dams in mountain valleys. These relatively small dams may also bring negative disastrous effects. As Zhou et al., 2013b pointed out, under certain inflow conditions, the dam in the channel will have a cascading collapse effect, resulting in collapsed debris flow or enlarging the discharge of debris flow, such as the 2010 Tangfanggou debris flow in Pingwu County and July 2013 Qipangou debris flow in Sichuan Province of China (Liu et al., 2010; Qin et al., 2016). Therefore, it is of great significance to analyze and evaluate the stability of landslide dams for the identification and mitigation of the landslide-debris flow disasters.

There are many factors that affect the stability of landslide dams. Among them, material distribution characteristics and geometric parameters of the dam body are the main internal factors which affect the permeability and mechanical properties of the dam body, thus determining the stability and failure mode of the dam (Costa and Schuster 1988; Casagli et al., 2003; Dunning, et al., 2005; Dunning, 2006; Shan et al., 2020; Zheng et al., 2022). The accumulation characteristics of landslide dams were mainly studied by means of survey statistics, laboratory model tests, and numerical simulations. Casagli et al. (2003) analyzed 42 landslide dams and found that the grain size gradation of the dam body appeared in double peaks. The median particle size d_{50} could not be used as a representative value of particle gradation. Chang et al. (2011) found that the parameters such as particle gradation, porosity, and plasticity index and other parameters of the dam material varied significantly with depth. Lei et al. (2016) studied the sliding and accumulation movement process of a cohesive soil slope along the inclined plane under unconfined conditions through model tests and found that factors such as volume of the slope, particle size, slope height, and slope angle of the start area have influences on the accumulation range and shape of the landslide debris dam. Peng et al. (2019) used the image recognition system PCAS to analyze the particle size distribution characteristics of the surface material of the landslide debris deposits in the Pusa Village collapse. Zhao et al. (2019) studied the effects of channel section shape, landslide velocity, and channel bed slope on the horizontal and vertical geometry of the dam based on the DEM. (Zhou et al., 2019a; Zhou et al., 2019b) studied the influence of the angle of the starting section, the angle and roughness of the sliding section on the morphology, and debris distribution of the deposits through model experiments and numerical simulations.

The aforementioned studies show that the debris distribution of landslide dams is complicated and the morphological features are also affected by many factors. However, most of the studies took the slope as homogenous and did not consider the influence of the structural characteristics of the slope body itself on the landslide damming process and accumulation characteristics. In addition, in natural conditions, it is difficult to directly know the internal structure and material composition of the dam in time because the formation of landslide dams is often sudden and difficult to reach (Wang et al., 2015). If the characteristics of the unstable slope in the source area can be linked with the accumulation characteristics of the landslide dam, we can quickly identify the characteristics of the dam by slope characteristics, which will provide a basis for rapid stability assessment and decision-making. Therefore, this study focused on the propagation and accumulation process of the landslide under different slope characteristics through physical model tests. The relationship between slope characteristics and accumulation characteristics of the dam was analyzed.

METHOD AND MATERIAL

Scaling

Model tests must consider scaling issues. According to the typical landslides in China since the 20th century reported by many researchers (Huang, 2007; Huang et al., 2008; Li et al., 2010), the ranges of typical landslide parameters are listed in **Table 1**. The length scale is selected as $\lambda_L = L_p/L_m = 500$, and the volume scale can be calculated as $\lambda_V = {\lambda_L}^3 = 1.25 \times 10^8$. For gravity-driven motion of landslides and debris flows, dynamic scaling involves a characteristic time scale $(L/g)^{1/2}$ (Iverson, 2015), where g is the magnitude of gravitational acceleration and L is the characteristic length of the moving mass. Then, the time scale for this study can be calculated as $\lambda_T = {\lambda_L}^{1/2} = 22.4$.

The comparison of model and prototype parameters is listed in **Table 1**.

Experiment Apparatus

A rotatable start-up landslide device was especially designed, as displayed in **Figures 1A–C**. The device was divided into three parts: starting section, sliding section, and accumulating section. The starting section simulated the sliding source area, which consisted of the rear wall, two side walls, and a rotatable bottom plate. The inclination of the rear wall was 50°, and the side walls were vertical with a height of 100 cm. The rotatable plate was 71 cm long and 67 cm wide. The inclination of the rotatable plate was set to 50° when it connected with the sliding section. The sliding section was a rectangle channel. It comprised two glass side walls and a steel bottom. The length of the channel was 230 cm, and the inclination was 30°. The accumulating section was designed as a narrow channel to form the landslide debris dam. The dimension of the channel was 400 cm (length)×26.5 cm (width)×30 cm (height). A transparent glass plate was installed on the side away from the sliding section. Three cameras were installed to record the process of initiation, propagation, and accumulation of the landslide. A 3D laser scanner was used to scan the geometry of the entire damming body.

Material and Test Conditions

This study mainly considered variables of the slope body features including types of material, slope accuracy, and layer sequence. The slope comprises three different kinds of debris, that is, coarse

TABLE 1 | Prototype and model parameters for the experiments (length scale $\lambda_L = L_p/L_m = 500$).

Items	Parameters	Prototype	Model	Specific value for the tests
Slope body	1) Vertical height(m)	200–900	0.4–1.8	0.15–0.2
	2) Slope angle (°)	10–40	10–40	34.9–45.6
Sliding bed	1) The length of the sliding bed(m)	200–2,450	0.4–4.9	3.0
	2) The width of the sliding bed (m)	100–1,500	0.2–3.0	0.67–0.77
	3) Source area inclination (°)	22–75	22–75	50
	4) Sliding area inclination (°)	18–45	18–45	30
Sliding body	1) Vertical distance (m)	190–1,500	1.0–10	1.72
	2) Horizontal distance (m)	400–1900	0.8–3.8	2.41
	3) The volume (m^3)	$(0.9–742)\times10^7$	0.072–59.4	0.012–0.325
Time	Duration(s)	<300	<13.4	<5

Note: Considering the safety and operability of the device, the height of the slope and the volume of the sliding body have been appropriately reduced. Since the prototype data were all derived from well-documented super-large landslides, there are more relatively small-scale landslides in nature, so it is reasonable to reduce them appropriately.

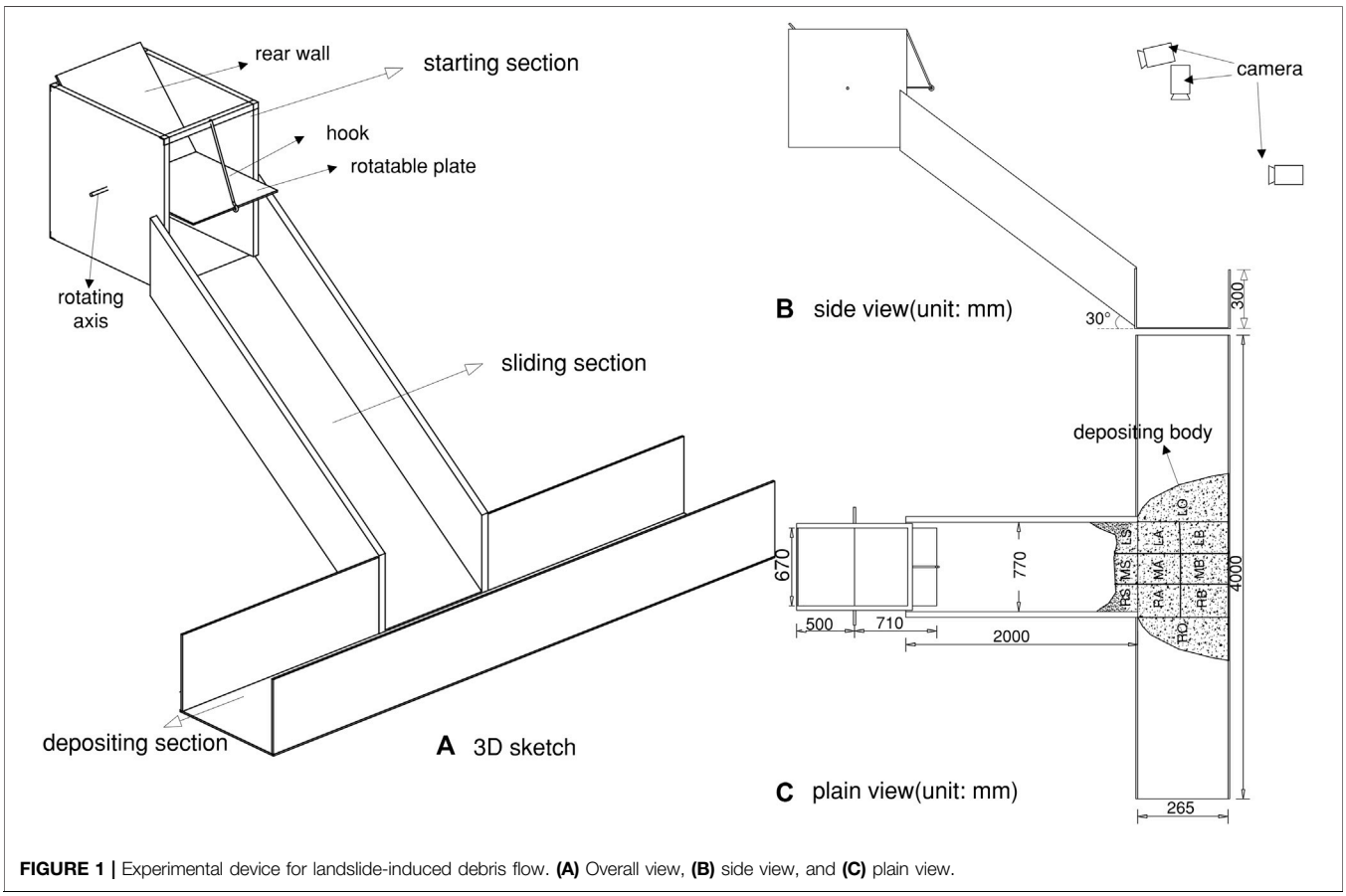

FIGURE 1 | Experimental device for landslide-induced debris flow. **(A)** Overall view, **(B)** side view, and **(C)** plain view.

gravel, medium gravel, and fine sand, as shown in **Figure 2**. The physical parameters of the material are shown in **Table 2**. In addition, all the coarse gravels were equally divided into three parts and colored red, green, and blue lacquer. They were used as tracers after the lacquer was completely dry.

The slope occurrence included uniform slope and layered slope. The uniform slope was made of the mixture of the three kinds of debris, as sketched in **Figure 3A**. The layered slope can be further divided into two types according to the relationship between the stratum surface and sliding surface. One was a parallel slope, which is referred to the stratum surface parallel to the sliding surface (**Figure 3B**). The other was an intersecting slope representing that the stratum surface was intersecting with the sliding surface (**Figure 3C**). As **Figure 3** showed, different strata were coded by Arabic numerals 1, 2, and 3. Different stratum sequences could be obtained by changing the types of materials at different layers. All the test conditions by combining these variables are listed in **Table 3**.

TABLE 2 | Physical and mechanical parameters of the material used in the tests.

Types of material	Diameter (mm)	Bulk density (kg/m^3)	Water content (%)	Total mass (kg)	Bulk volume (×10^{-3}m^3)	Friction angle (°)
C[a]	20–40	1,690	1.2	20	11.8	36.8
M[b]	5–10	1,562	1.3	20	12.8	33.1
F[c]	<0.5	1,405	1.5	20	14.2	30.9

Note:
[a]*C, coarse gravel.*
[b]*M, medium gravel.*
[c]*F, fine sand.*

FIGURE 2 | Material samples for the model tests.

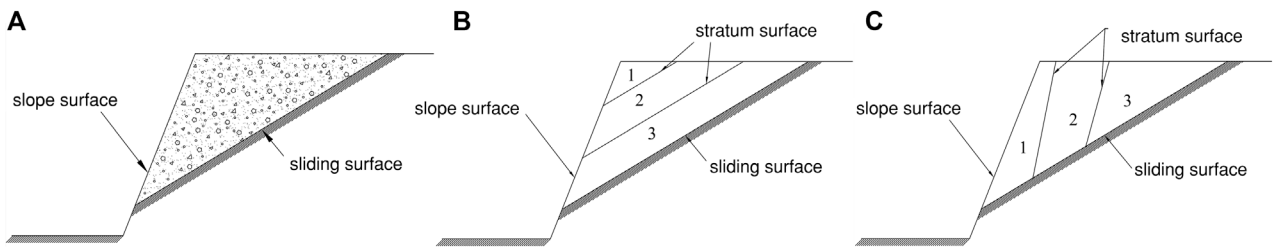

FIGURE 3 | Schematic of the slope structure **(A)** uniform slope; **(B)** parallel slope, that is, stratum surface paralleling with the sliding surface; **(C)** intersecting slope, that is, stratum surface intersecting with the sliding surface. The numbers 1, 2, and 3 are stratum sequence codes.

Test Procedure and Measurements

1) The entire test device is cleaned up, and the rotatable plate is fixed in the horizontal position.
2) The slope body model is constructed; In order to stimulate the layered slope body, we placed the slope body in the horizontal position first and then released the rotatable plate to form a slope body in an inclined state. It is easy to construct a uniform slope body by just putting the fully mixed debris on the horizontal plate and then rotating the plate to form an inclined uniform slope. However, it is a bit more complete to make the layered slope model. Different debris are stacked horizontally from the bottom to top and laterally from the rear wall to the free surface to form a parallel slope and intersecting slope, respectively, as shown in **Figures 4A1,A2**. The tracers were carefully placed as shown in **Figures 4B1,B2**. The initial slope body was basically kept complete during the rotating process because of the inertia and was not really started until the plate rotated to the designed position. The slope angle for the horizontal state slope is the particle repose angle and is approximately equal to the sum of the plate inclination and repose angle when in the inclined state.
3) The accumulation width and depth of different materials in the landslide dam is recorded, and the geometric characteristics of the entire deposition are scanned with a 3D laser scanner.
4) Areas of the deposition and sampling, sieving, and weighing the materials are divided in each corresponding area. The plain view of the subareas of the dam is shown in **Figure 1C**. Along the longitudinal direction (along the valley), it was divided into the main accumulation body corresponding to the width of the sliding section and the expansion on both

TABLE 3 | Test conditions.

Slope feature code	Slope occurrence	Stratum sequence			Tracer particle distribution
		Coarse gravel (C)	Medium gravel (M)	Fine sand (F)	
M-CMF	Uniform mixed	-	-	-	-
P-CMF	Parallel	1	2	3	Longitudinal[a]
P-FMC		3	2	1	Longitudinal
P-MCF		2	1	3	Longitudinal
P-CFM		1	3	2	Transverse[b]
P-MFC		3	1	2	Transverse
P-FCM		2	3	1	Transverse
I-CMF	Intersecting	1	2	3	Longitudinal
I-FMC		3	2	1	Longitudinal
I-MCF		2	1	3	Longitudinal
I-CFM		1	3	2	Vertical[c]
I-MFC		3	1	2	Vertical
I-FCM		2	3	1	Vertical

[a]*Longitudinal distribution of the tracer particles in the slope body means the tracers were displayed along the valley direction, as shown in* ***Figure 4B1,I*** *and* ***Figure 4B2,III****.*
[b]*Transverse distribution in parallel slope means the tracers distributed from the rear wall to free surface* ***Figure 4B1,II****.*
[c]*Vertical distribution in the intersecting slope indicated that the tracers distributed from the top to the sliding surface of the slope* ***Figure 4B2,IV****.*

sides. The main accumulation body was further equally divided into left (L), middle (M), and right (R) sub-areas, and the expansion included left outer (LO) and right outer (RO) sub-areas. In the sliding direction, we only sub-divided the main accumulation body into the slope toe area (S), near slope area (A), and far away slope area (B). In the vertical direction, the main accumulation body was equally divided into the upper layer (U) and the lower layer (D) according to its thickness.

RESULTS AND DISCUSSION

Accumulation Characteristics of Landslide Debris Dam

Morphology of the Landslide Dam

It is obvious from **Figures 5A,B** that the damming bodies formed under different slope conditions were basically similar in plain view and longitudinal section. Most of the material accumulated in the main channel, which was fan

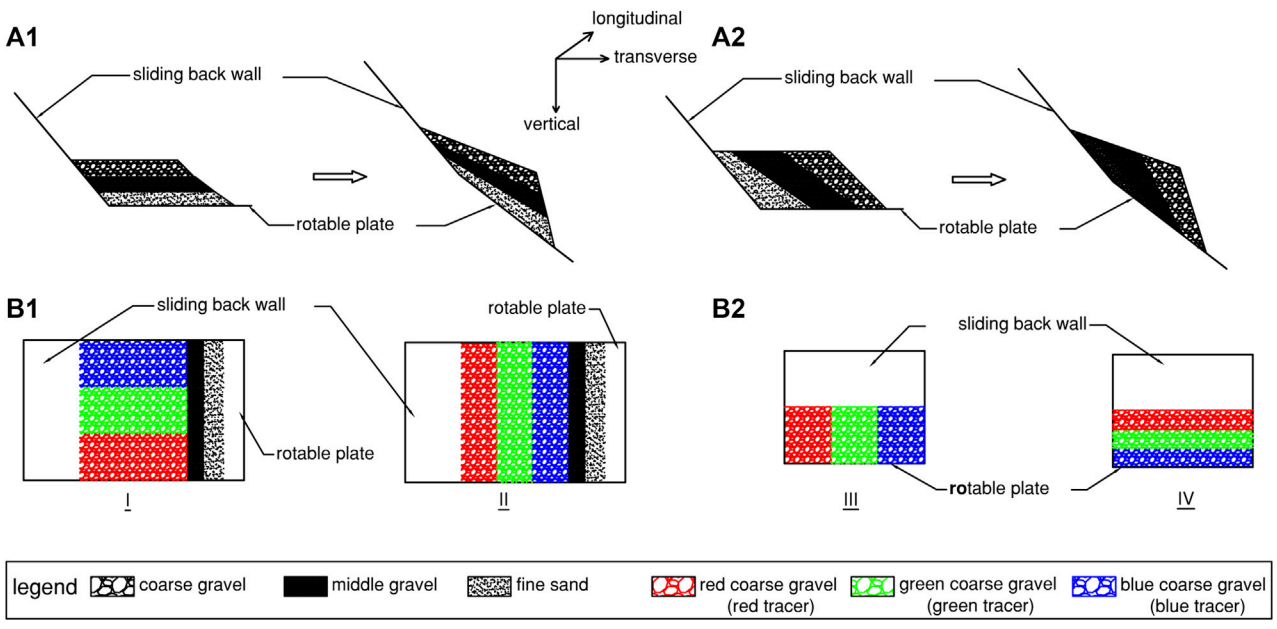

FIGURE 4 | Schematic diagram of slope-making and the distribution of tracer particles; **(A1)** the method of making a parallel slope, taking the P-CMF as an example; **(A2)** the method of making an intersecting slope, taking the I-CMF as an example **(A)**; **(B1)** the plain view of the tracer particle distribution in the parallel slope, in which I displays longitudinal distribution and II transverse distribution; **(B2)** the front view of the tracer particle distribution in the intersecting slope, in which III displays longitudinal distribution and IV vertical distribution.

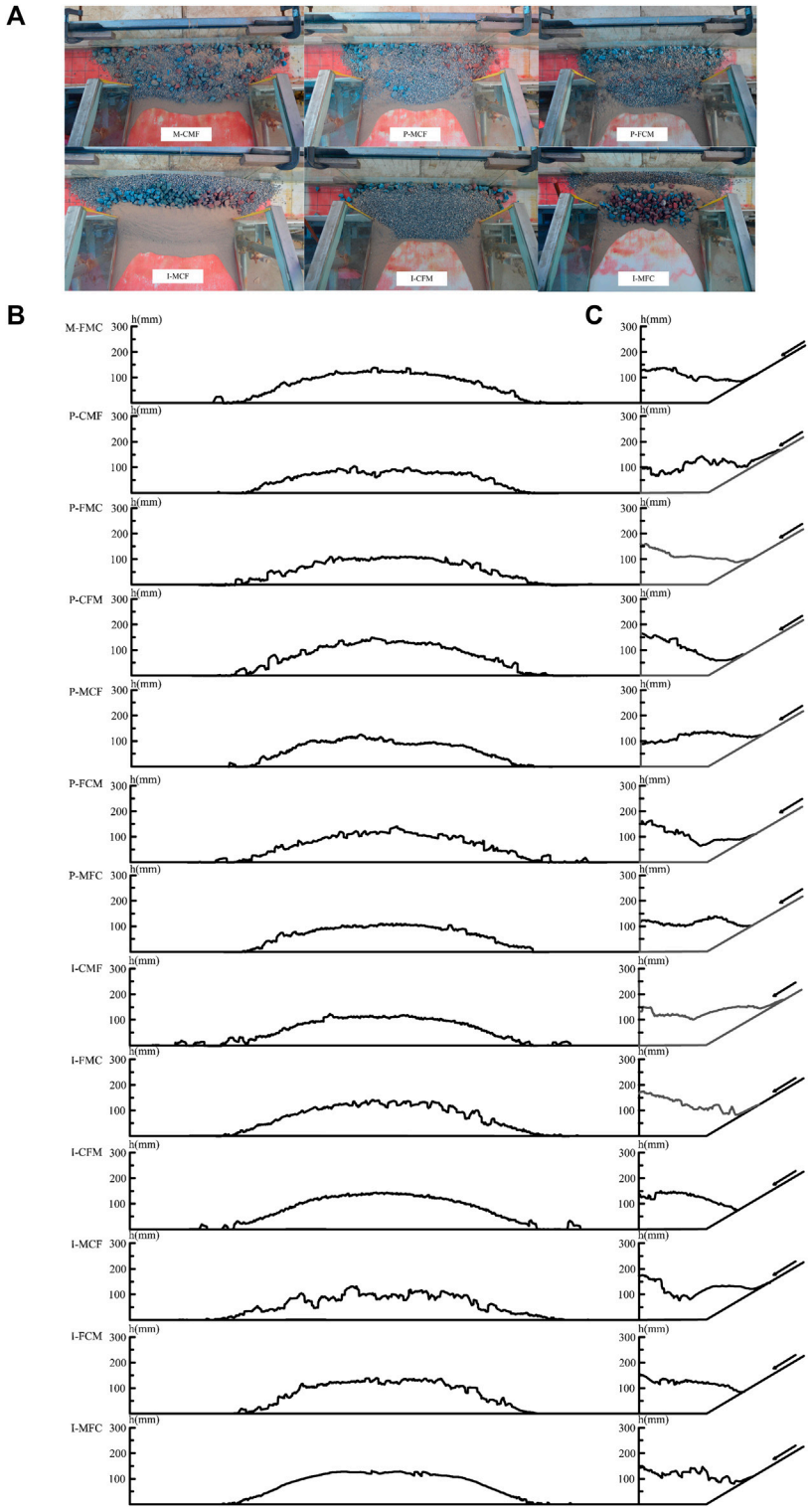

FIGURE 5 | Profiles of the landslide debris dams under different slope conditions. **(A)** Plain view; **(B)** longitudinal section; **(C)** cross section.

plain–shaped; a small amount of the material deposited on the bottom of the slope, which was saddle-shaped, and the saddle shape formed by the oblique slope was the most obvious. The longitudinal cross-section of the dams was of symmetrical parabolic shape, and the inclination angle on both sides was about 13°–16°.

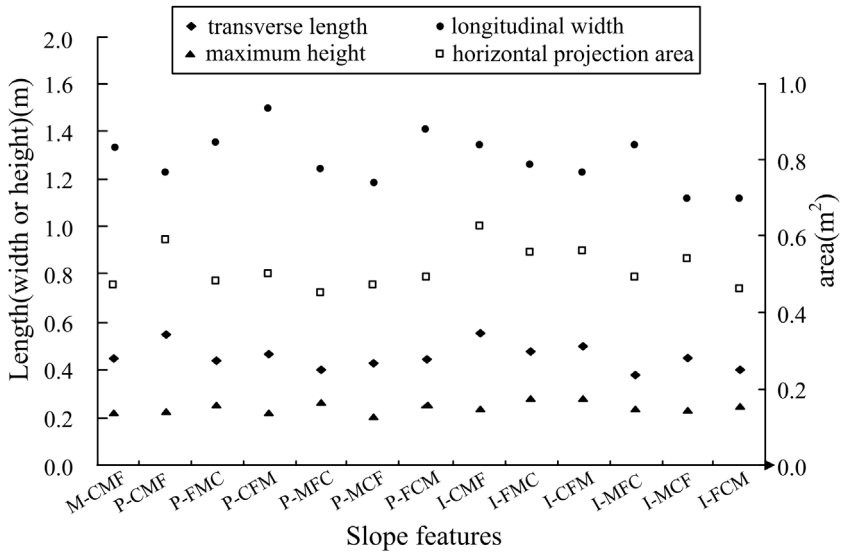

FIGURE 6 | Morphological parameters of the landslide debris dam under different conditions.

However, **Figure 5C** showed that the cross-section shapes of the dams formed by different slopes were quite different. Under the condition of uniform slope, the shape of the cross section was relatively flat, with the front part slightly higher than the rear part. However, it varied dramatically under the conditions of layered slopes. In general, the morphology of the cross section can be divided into three types: 1) the flat pattern, as the typical examples of P-MCF and P-MFC. The overall profile of the cross section was relatively flat without obvious undulations, and the average inclination angle from the front edge to the tail of the accumulation was less than 10°; 2) unidirectional inclined pattern, such as the condition of P-CFM and I-FMC. The inclination direction was mostly toward the sliding bank, and the inclination angle from the front edge to the tail of the accumulation was about 10–20°; 3) undulating pattern: it showed that the profile of the entire cross section presented large fluctuations. Specifically, it could be further divided into two-segment type (e.g., P-FCM, P-FMC, I-FCM, and I-MCF) and multi-segment type (e.g., P-CMF and I-CMF).

Figure 6 showed the morphological parameters such as longitudinal bottom width (W_{bd}), transverse length (L_d), maximum height (h_{max}), and horizontal projected area (A_d) of the landslide dam under different conditions. The geometric parameters of the dam were also different with the difference of the stratum sequence in parallel slopes and intersecting slopes. The longitudinal width of the dams formed by the parallel slope was generally larger than that of the intersecting slope. The distribution of the transverse length and horizontal projected area was basically the same; the maximum height did not change much, but there was a difference in its position according to **Figure 5C**. Among these parameters, the longitudinal width altered the most, indicating that it was affected most by the stratum sequence.

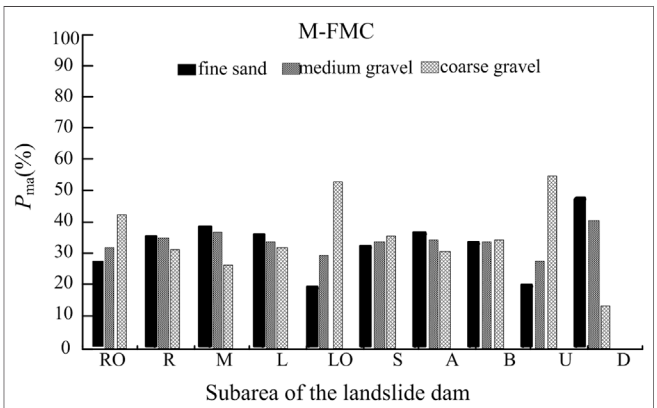

FIGURE 7 | Distribution characteristics of material composition in the dam formed by the uniform slope.

Material Distribution of Landslide Dam

We can intuitively observe from **Figure 5A** that there were obvious differences in the material distribution of the dams formed by different slopes. The sieving data are used to calculate the percentage of different materials in each area to the total substance in the area (P_{ma}) for further analysis. **Figure 7** showed that along the longitudinal direction in the dam formed by the uniform slope, the content of coarse gravel was relatively the largest in the outer expansion area, and the content of each material in the main deposit areas was pretty much the same; in the sliding direction, the three kinds of material in each area distributed more evenly, with P_{ma} more than 30%; in the vertical direction, the largest content in the upper layer was fine sand, followed by medium gravel, and coarse gravel consequently and vice versa in the layer below.

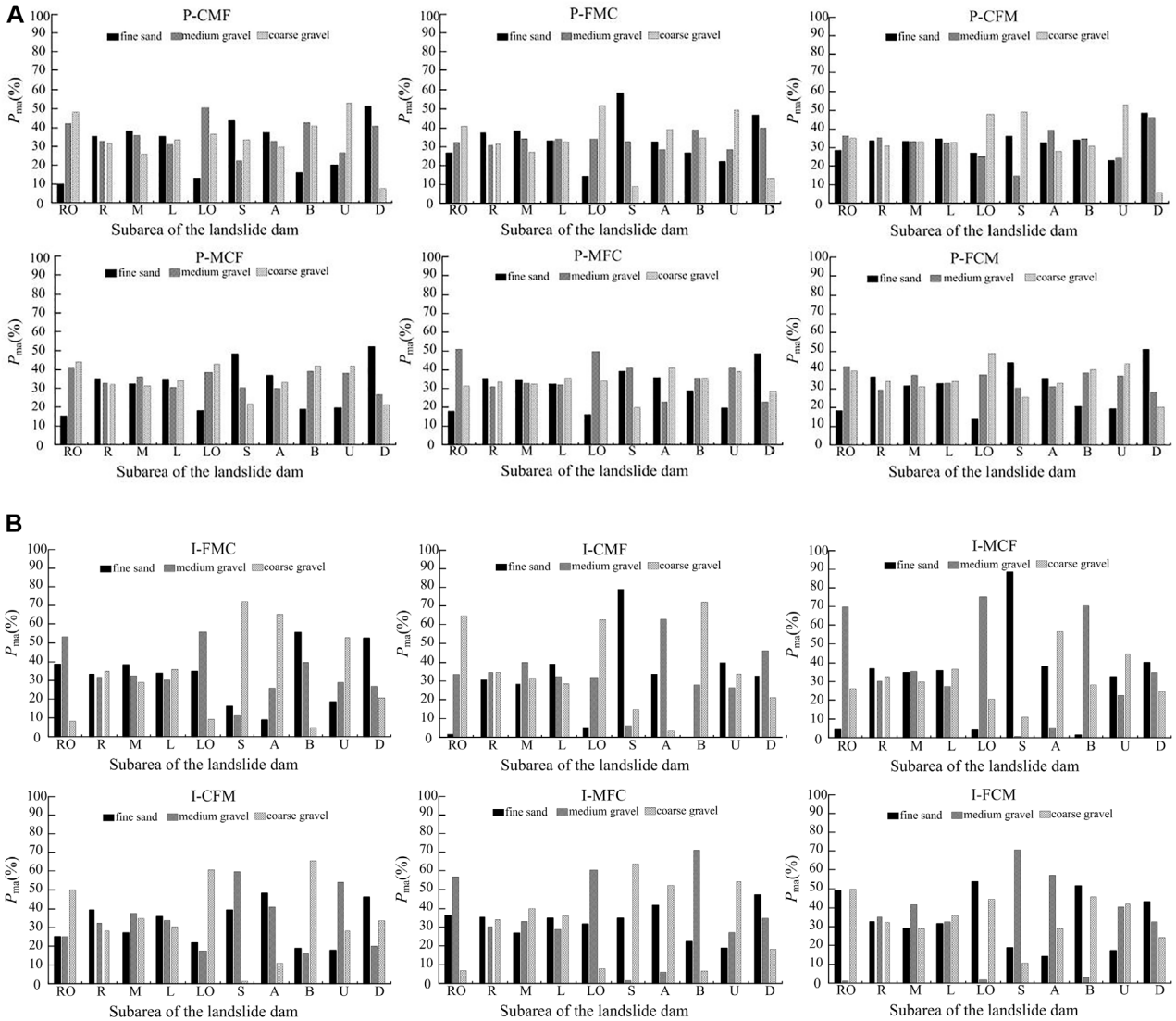

FIGURE 8 | Distribution characteristics of material composition in the dam formed by the parallel slope and intersecting slope. **(A)** Parallel slope. **(B)** Intersecting slope.

This phenomenon was called the inverse grading according to Heim (1932).

Figure 8A demonstrates that the material distribution characteristics of the dam formed by parallel slopes were basically similar to those of the uniform slope in the longitudinal and vertical directions. In the sliding direction, the feature of fine particles prevailing in the area of *S* and coarse particles in the area of *B* could be observed, which indicated a regularity that coarse particles move much farther than fine particles.

Figure 8B shows that the material distributions of the dam formed under various conditions of the intersecting slope were quite different compared with those of the uniform slope and the parallel slope. In the longitudinal direction, the substances located in the 1st^{s} layer of the slope were most abundant in the outward expansion areas (LO and RO), and the distribution of the substances in the main accumulation areas (L, M, and R) was relatively uniform. In the sliding direction, the most abundant material in the S, A, and B areas always came from the 3rd, 2nd, and 1st layers in the slope body respectively, which indicated that the material distribution of the dam was consistent with the material distribution of the slope body. In the vertical direction, the contents of medium and coarse gravel in the upper layer were greater than those of fine sand under some working conditions (I-FMC, I-MFC, I-MCF, and I-FCM), which basically met the inverse grain distribution characteristics. But, for the condition of I-CMF, the contents of fine sand were greater than those of coarse gravel in both the upper layer and lower layer. This could be explained by the sorting mechanism in the process of movement and accumulation.

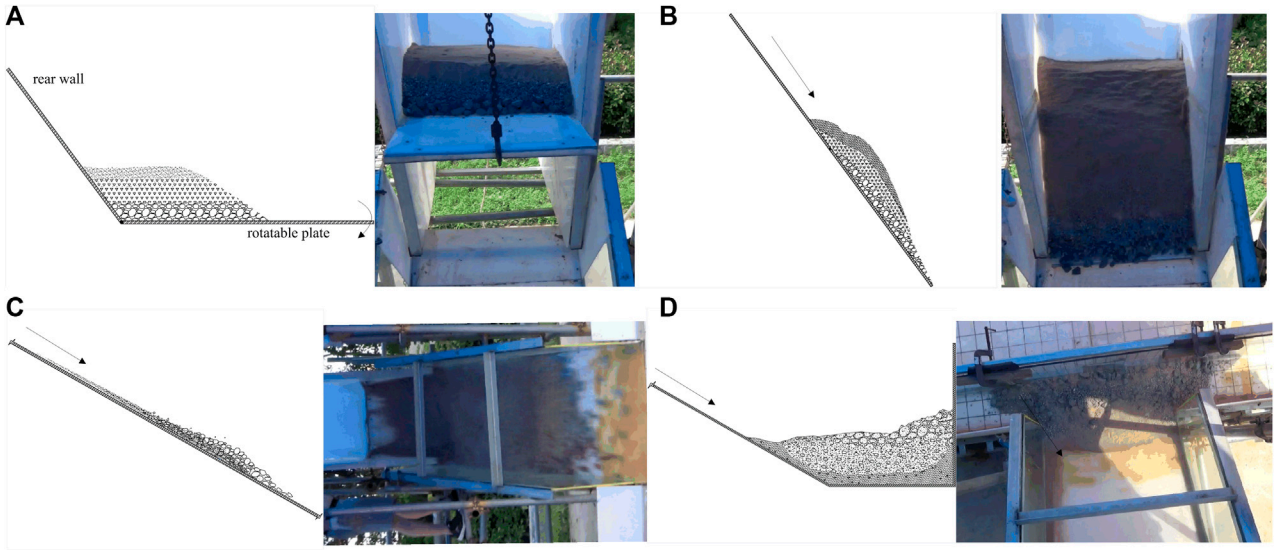

FIGURE 9 | Damming process of a landslide under parallel slope conditions (e.g. P-FMC). **(A)** Initial state of the slope body; **(B)** starting stage; **(C)** sliding stage; and **(D)** depositing stage.

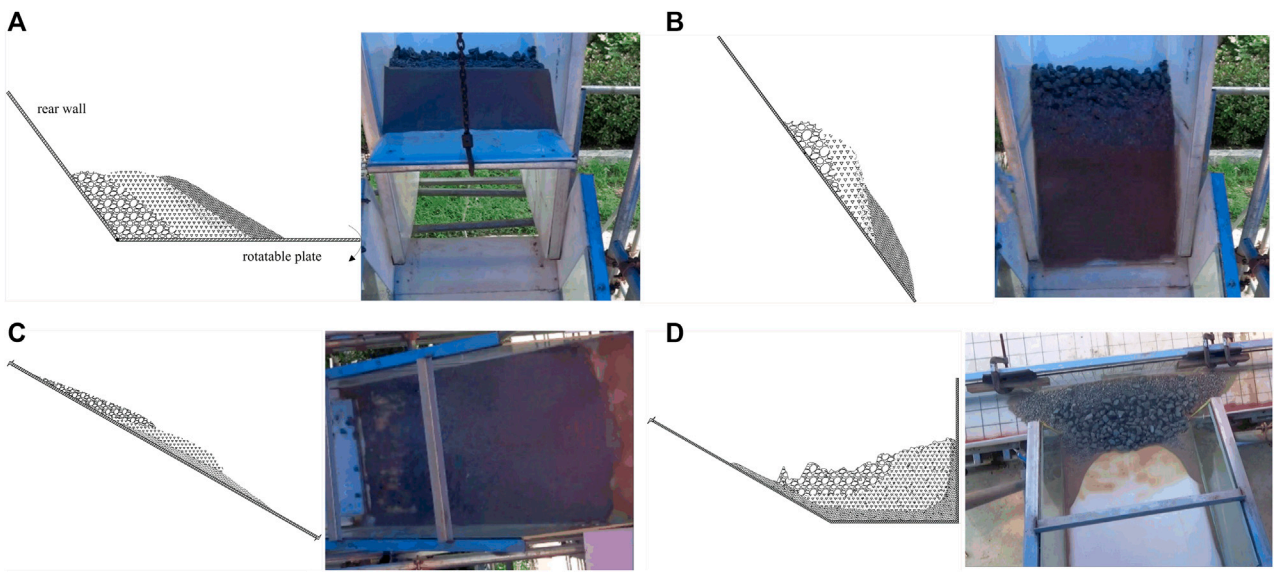

FIGURE 10 | Damming process of a landslide under intersecting slope conditions (e.g. I-FMC). **(A)** Initial state of the slope body; **(B)** starting stage; **(C)** sliding stage; **(D)** depositing stage.

Accumulation Mechanisms of Landslide-Debris Dams

Dynamic Process of Landslide-Debris Dams

The characteristics of the propagation and accumulation under different slope conditions were different. In general, it could be divided into three stages:

(1) The rotating–starting stage: It refers to the process where the rotatable plate rotated from a horizontal state to the designed angle and caused the material to start, with an average time of 0.36–0.4 s. This stage could be sub-divided into a rotating process and starting process based on the motion state of the slope body. The rotating stage refers to the process of rotating, which lasted 0.24 s. In the rotating process, the overall shape of the slope body was kept complete, and no obvious sliding appeared. The debris started to slide due the vibration of the rotatable plate contacting with the sliding bed and gravity. Two typical starting modes of the slope body were observed in different slope conditions. Visible overall depression and deformation can be observed in the uniform

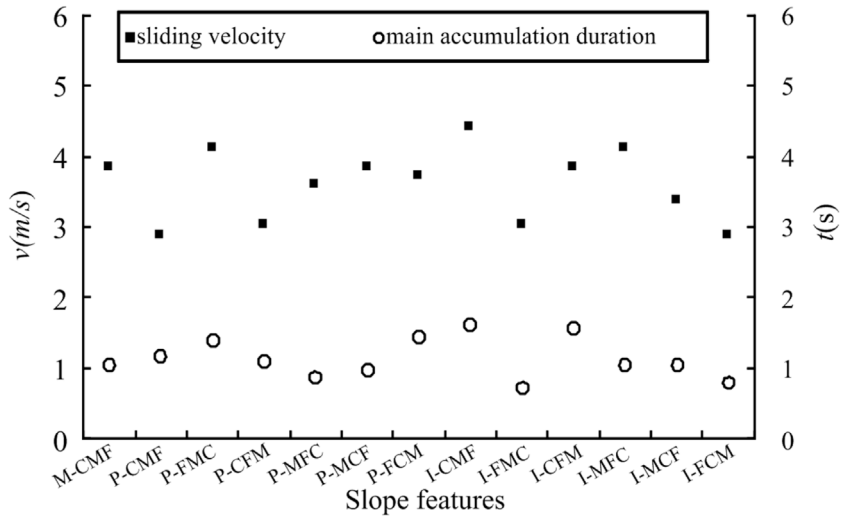

FIGURE 11 | Average velocity and accumulation stage duration of a landslide under different slope conditions.

and parallel slope body, as shown in **Figures 9A,B**, which demonstrated an overall initiation mode of the slope body. However, a layered initiation mode was observed in the intersecting slopes. The debris at the 1st stratum declined apparently with no obvious movement in the 2nd and 3rd strata (**Figures 10A,B**).

(2) The sliding stage: It refers to the stage where the faucet of the sliding body moves in the sliding section. For uniform slopes and parallel slopes, the faucet of the sliding body mainly comprised coarse particles, with a mixture of the three kinds of debris in the middle and fine sand in the tail, as shown in **Figure 9C**. However, the faucet of the sliding body only comprised the debris in the 1st stratum for the intersecting slope conditions, and the 2nd and 3rd strata started and moved successively (**Figure 10C**). The average velocity of the sliding stage varied from 3.0 m/s to 4.4 m/s under different slope conditions, as shown in **Figure 11**. The tongue-like cross section of the sliding body indicated that the middle moved faster than both sides.

(3) The depositing stage: This stage starts from the accumulation of the sliding body faucet until all the debris accumulated, which could be sub-divided into the main channel accumulation stage and slope accumulation stage. The faucet of the sliding body moved to the accumulation area and stopped when it encountered the valley bank. The debris that arrived subsequently quickly rose and spread to both sides, forming a fan-shaped accumulation body; a small amount of the materials accumulated at the foot of the slope, and the fine sand near the side wall of the sliding bed continued to slide down, eventually forming a saddle-shaped tail, as shown in **Figures 9D**, **10D**.

Vertical Infiltration Under Parallel Slope

Figure 11 showed that the average velocity of the sliding stage and the duration of the accumulation stage varied greatly under different slope conditions. The largest velocity appeared in the condition of I-CMF, followed by P-CMF and M-FMC, which indicated that the coarser the faucet of the sliding body, the faster the moving speed, and the larger average velocity of the sliding stage. As is elaborated previously, the faucet of the sliding body for I-CMF only comprised coarse gravel, while the other two counterparts consisted of a mixture of different debris. The mixture of the parallel slope was formed by the vertical infiltration effect, which means that fine debris at the upper layer penetrated to the lower layer when making a parallel slope model and during movement, thus causing a certain mixture at the 3rd layer.

Further analysis of the sliding velocity of different parallel slope conditions implies that even the debris at the 3rd layer was the same particle; the sliding velocity was different when the fine sand is at a different layer. The velocity was generally smaller when the content of fine sand at the 2nd layer was greater than that at the 1st layer, such as P-MFC < P-FMC and P-CFM < P-FCM. This further verified the vertical infiltration effect of fine particles to the coarse particles during the damming process. The closer the fine sand was to the 3rd layer, the more it penetrated down to the 3rd layer, and the greater effect the slowing on the movement speed. Vertical infiltration not only affected the sliding velocity but also caused inverse grading in material distribution of the dam.

Pushing–Climbing Effect and laterial Infiltration Under Intersecting Slope

Figure 11 also showed that the shortest and longest duration of the accumulation stage was I-FMC and I-CMF, respectively, which all belonged to the inclined slope. The fine and coarse particles moved and accumulated successively under the condition of I-FMC. The coarse gravels with the largest velocity at the end exerted a pushing effect to the medium gravels in front, and the medium gravels in turn pushed the fine sand. The progressive pushing effect between different debris accelerated the entire sliding and accumulating process.

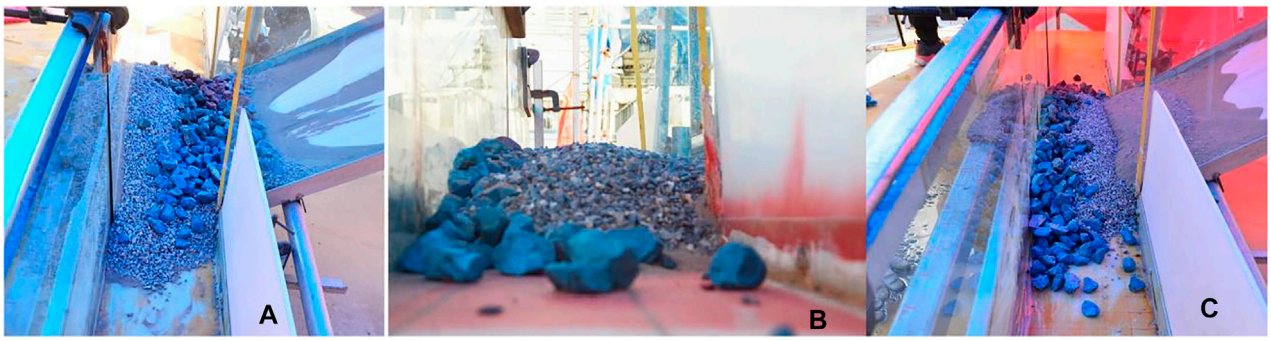

FIGURE 12 | Landslide debris deposits under intersecting slope with different sequences. **(A)** I-FMC with an obvious pushing–climbing effect; **(B)** I-CFM with strong horizontal infiltration; **(C)** I-CMF without obvious an pushing–climbing effect.

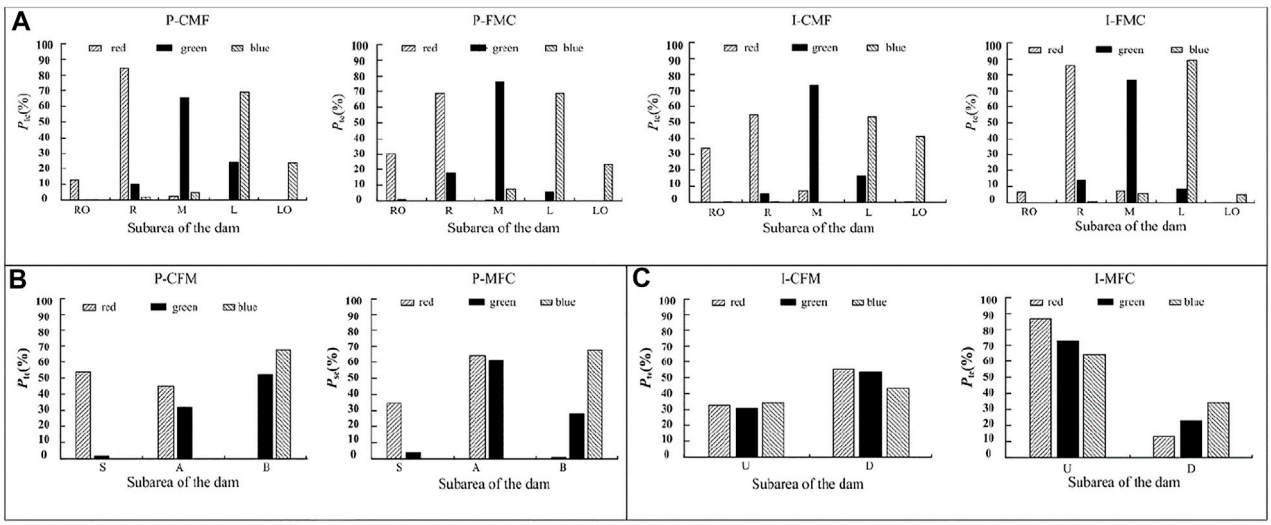

FIGURE 13 | Distribution of tracer particles in different areas of landslide dams under different distributions in the slope body. **(A)** Tracer particle distributed along the longitudinal direction in the slope; **(B)** tracer particle distributed along the transverse direction in the parallel slope; **(C)** tracer particle distributed along the vertical direction in intersecting slope. The parameter P_{ts} represented the mass percentage of different tracer particles in each area of the dam to the total amount of each kind of tracer particles.

In addition, due to the larger velocity of the coarse particles, the coarse particles climbed up and accumulated on the top of the fine particles, resulting in a large overlapping area of the dam in the vertical direction (see **Figures 10D**, **12A**). This is the main reason why the dams formed by some intersecting slopes presented the inverse grading distribution regularity.

In addition to this, the pushing effect can also make the dam more compact. **Figure 6** displayed that the transverse length of the dam body with the pushing effect in the damming process was generally low, such as I-CFM, I-MFC, and I-FCM. Among the aforementioned conditions, the transverse length under the condition of I-CFM was the lowest, which indicated another mechanism—lateral infiltration. The fine sand penetrated much into the voids of the coarse gravel in front due to the pushing effect exerted by the medium gravel behind. As a result, little fine sand could be observed in the dam from the side view as shown in **Figure 12B**. As for I-MFC, the lateral permeability of the fine sand reduced significantly because the porosity of the medium gravel was apparently lower than that of the coarse gravel so that the transverse length was relatively larger than that of the I-CFM.

On the contrary, the coarse particles and fine particles started moving successively under the condition of I-CMF (see **Figure 12C**). The coarse particles moved ahead and faster than the fine particles. Neither the pushing effect nor the lateral infiltration effect was obvious during the damming process, resulting in the longest duration of the accumulation and the longest distance of the transverse length of the dam. As different debris stacked mainly side by side in the sliding direction, the content of the upper and lower layers of each kind of debris was not much different. Due to the different repose angles of the materials, there was obvious fluctuation at the junction of different materials,

which was manifested as obvious multisegment undulations in the transverse cross section (**Figure 5C**).

DISCUSSION

Accumulation Characteristics of Landslide Dam

The cross-section morphology of landslide dams has an important influence on the mechanism of dam breach. The lowest point of the cross section determines the location of the initial breach and the erosion pattern (Zhao et al., 2019). Numerous studies have reported that the cross-sectional shape of a landslide dam is affected by the topographic and morphological conditions such as the starting section angle, inclination of the sliding section, distance and roughness of the sliding bed, shape of the depositing channel, and volume of the sliding body (Okura et al., 2003; Di Luzio et al., 2004; Wang, et al., 2012; Zhao et al., 2017; Crosta et al., 2017; Zhao et al., 2019; Zhou et al., 2019a; Zhou et al., 2019b). However, under the same topography, morphology, and volume conditions in this experiment, the cross-sectional shapes of the dams are also quite different due to different slope structure. The cross-sectional morphology that appears in this experiment includes almost all morphologies mentioned in the studies of Zhao et al. (2019) and Zhou et al., (2019a), which demonstrate that the geometrical morphology of landslide dams is not only affected by the topography but also by the geological conditions of the slope body.

The material distribution characteristics of landslide dams affect the permeability and mechanical properties of the dam. Previous studies have concluded some rules for the material distribution characteristics of landslide deposits. It is generally believed that there is an inverse grading along the vertical direction in landslide debris dams (Savage and Lun, 1988; Zhou and Ng, 2010; Zhang and Yin, 2013; Gray, 2018). Many researchers proposed different hypotheses to explain the mechanism, such as the dispersive pressure proposed by Bagnold (1956) that made the coarse particles move to the debris flow surface. The kinematic sieving during the movement also contributed to the sorting (Zheng et al., 2019). This study basically yielded the same results of inverse grading distribution, but with different sorting mechanisms under different slope conditions. For the uniform and parallel slopes, obvious inverse grading distribution is induced by overall initiation of the slope body and strong vertical infiltration of the fine sands during the movement. However, inverse grading distribution is generated by the effects of pushing–climbing, and lateral infiltration existed among particles.

Relationship Between Material Distribution Characteristics of the Landslide Dam and Slope Body

By analyzing the distribution of tracer particles, we could easily obtain a conclusion that the debris distributed longitudinally in the slope is mainly accumulated in the corresponding longitudinal area of the dam, as shown in **Figure 6** of P-MCF and I-MCF. **Figure 13A** further demonstrated that about 70–80% of the tracer particles slide to the corresponding areas of the dam and 10–30% to the adjacent areas on both sides. There was no cross-regional distribution phenomenon, that is, no green tracer particles from the middle of the slope were found in the outer expansion areas of the dam, and no blue tracer particles from the left side of the slope appeared in the right side of the dam and vice versa. **Figure 13B** indicated that the tracer particles distributed transversely in the slope body accumulated in the corresponding area of the dam along the sliding direction, which was also illustrated by **Figure 5A**P-FCM. However, different tracer particles distributed vertically in the intersecting slope appeared randomly in the vertical direction of the dam, and it was even affected by the layer sequence of the tracer particles in the slope. For I-CFM, the mass percentages of different tracer particles in the lower part of the dam were all greater than those in the upper part. About 60% of the red tracer located in the upper part of the slope body accumulated in the lower part of the damming body (**Figure 13C** I-CFM), while more tracer particles located in the upper part of dam when the tracer particles were at the 3rd layer, as shown in **Figure 5A** I-MFC and **Figure 13C** I-MFC. This phenomenon indicated that there was a vertical exchange of the same particles in the process of damming, which was consistent with the study by Umbanhowar et al. (1998).

Although we elaborated the accumulation characteristics of the landslide dam formed by different slope conditions and discussed the relationship between the accumulation characteristic of the landslide dam and the slope body and analyzed the sorting mechanism, further research is still needed on the mechanism from the perspective of mechanics.

CONCLUSION

Through the model tests, we investigated the damming process of the landslide debris dam under different slope characteristics and analyzed the morphological characteristics and composition distribution characteristics of the dams. The main conclusions are listed as follows:

1) The morphological characteristics of the landslide debris dam are regulated by the slope structure, especially for the transverse cross-sectional shape. Three typical cross-sectional shapes are obtained: flat, unidirectional inclined, and undulating shapes. The cross section of the dam formed by the uniform slope is flat. The dams formed by the parallel slopes mostly present flat or unidirectional inclined cross-sectional shape, while undulating shapes occur for the intersecting slopes.
2) The debris distribution of the landslide dams is also affected by the slope body features. The debris grains are relatively uniformly distributed in the longitudinal and sliding directions of the dams formed by the uniform slope, but an obvious inverse distribution appears in the vertical distribution. The debris distributions of the dams formed by the parallel slopes are similar in the longitudinal and vertical direction but show a bimodal structure where fine gravel is close to the slope and coarse gravels are far away from

the slopes. The debris distributions of the dams formed by the intersecting slopes depend on the stratum sequence.

3) The debris distribution of the landslide dam is closely related to the debris structure of the slope body. Debris distributed in the longitudinal and transverse directions of the slope body is located in the longitudinal and sliding regions of the dam body. However, debris along the vertical direction of the slope body is weakly correlated with the debris in the vertical direction of the dam due to a vertical exchange effect.
4) The damming process and sorting mechanisms are affected by slope structure. The debris grains are well mixed for the uniform and parallel slopes during the movement process. The inverse distribution of the dam in the vertical direction is caused by the vertical infiltration effect of fine particles during the movement process. The original stratum sequence is maintained for the intersecting slope with layered debris during the movement and accumulation process. Due to the successive initiation of fine and coarse gravels, the effects of pushing–climbing and lateral infiltration among the particles are generated, leading to a larger sliding velocity and shorter accumulation duration. Thus, an inverse distribution in the vertical direction of the dams occurs.

DATA AVAILABILITY STATEMENT

The original contributions presented in the study are included in the article/Supplementary Material, further inquiries can be directed to the corresponding author.

AUTHOR CONTRIBUTIONS

XX and XW contributed to the conception and design of the study. SZ, ZL, XW, XQ and SX carried out all the experiments, XX, SZ and ZL organized the database. XX performed the statistical analysis and wrote the first draft of the manuscript. All authors contributed to manuscript revision and read and approved the submitted version.

FUNDING

This work is supported by the National Natural Science Foundation of China (Grant No. 41907258) and Doctoral Research Start-up Fund of Anyang Institute of Technology (BSJ2019011).

REFERENCES

Bagnold, R. A. (1956). The Flow of Cohesionless Grains in Fluids. *Phil. Trans. R. Soc. Lond. Ser. A, Math. Phys. Sci.* 249 (964), 235.

Casagli, N., Ermini, L., and Rosati, G. (2003). Determining Grain Size Distribution of the Material Composing Landslide Dams in the Northern Apennines: Sampling and Processing Methods[J]. *Eng. Geology*. 69 (1/2), 83–97. doi:10.1016/s0013-7952(02)00249-1

Chang, D. S., Zhang, L. M., Xu, Y., and Huang, R. Q. (2011). Field Testing of Erodibility of Two Landslide Dams Triggered by the 12 May Wenchuan Earthquake. *Landslides* 8 (3), 321–332. doi:10.1007/s10346-011-0256-x

Costa, J. E., and Schuster, R. L. (1988). The Formation and Failure of Natural Dams. *Geol. Soc. America Bull.* 100 (7), 1054–1068. doi:10.1130/0016-7606(1988)100<1054:tfafon>2.3.co;2

Crosta, G. B, De Blasio, F. V, De Caro, M, Volpi, G, Imposimato, S, and Roddeman, D. (2017). Modes of propagation and deposition of granular flows onto an erodible substrate: Experimental, Analytical, and Numerical Study. *Landslides* 14, 47–68. doi:10.1007/s10346-016-0697-3

Di Luzio, E., Bianchi-Fasani, G., Esposito, C., Saroli, M., Cavinato, G. P., and Scarascia-Mugnozza, G. (2004). Massive rock-slope failure in the Central Apennines (Italy): the case of the Campo di Giove rock avalanche. *Bull. Eng. Geol. Environ.* 63 (1), 1–12. doi:10.1007/s10064-003-0212-7

Dunning, S. A., Petley, D. N., Rosser, N. J., and Strom, A. L. (2005). *The Morphology and Sedimentology of Valley Confined Rock-Avalanche Deposits and Their Effect on Potential Dam Hazard Landslide Risk Management*. London: Taylor and Francis Group, 691–701.

Dunning, S. A. (2006). The Grain Size Distribution of Rock-Avalanche Deposits in valley Confined Settings. *Ital. J. Eng. Geol. Environ.* 1, 117–121. doi:10.4408/IJEGE.2006-01.s-15

Fan, X., van Westen, C. J., Xu, Q., Gorum, T., and Dai, F. (2012). Analysis of Landslide Dams Induced by the 2008 Wenchuan Earthquake. *J. Asian Earth Sci.* 57, 25–37. doi:10.1016/j.jseaes.2012.06.002

Fan, X., Xu, Q., Alonso-Rodriguez, A., Subramanian, S. S., Li, W., Zheng, G., et al. (2019). Successive Landsliding and Damming of the Jinsha River in Eastern Tibet, China: Prime Investigation, Early Warning, and Emergency Response. *Landslides* 16 (5), 1003–1020. doi:10.1007/s10346-019-01159-x

Gray, J. M. N. T. (2018). Particle Segregation in Dense Granular Flows. *Annu. Rev. Fluid Mech.* 50, 407–433. doi:10.1146/annurev-fluid-122316-045201

Heim, A. (1932). *Landslides and Human Live*. Vancouver, B C: Bitech Publishers, 93–94.

Hu, X. W., Huang, R. Q., Shi, Y. B., Lu, X. P., and Wang, X. R. (2009). Analysis of Blocking River Mechanism of Tangjiashan Landslide and Dam-Breaking Mode of its Barrier Dam. *Chin. J. Rock Mech. Eng.* 28 (1), 181–189. doi:10.3321/j.issn:1000-6915.2009.01.024

Huang, R. Q. (2007). Large-scale Landslides and Their Sliding Mechanisms in China since the 20th century. *Chin. J. Rock Mech. Eng.* 26 (3), 433–454. doi:10.3321/j.issn:1000-6915.2007.03.001

Huang, R. Q., Pei, X. J., and Li, T. B. (2008). Basic Characteristics and Formation Mechanism of the Largest Scale Landslide at Daguangbao Occurred during the Wenchuan Earthquake. *J. Eng. Geology*. 16 (6), 730–741. doi:10.3969/j.issn.1004-9665.2008.06.002

Iverson, R. M. (2015). Scaling and Design of Landslide and Debris-Flow Experiments. *Geomorphology* 244 (sep.1), 9–20. doi:10.1016/j.geomorph.2015.02.033

Lei, X. S., Xie, W., Lu, K. L., Zhu, D. Y., and Chen, J. X. (2016). Model Tests of Sliding and Accumulation Characteristics of Cohesionless Soil. *Chin. J. Geotechnical Eng.* 38 (2), 226–236. doi:10.11779/CJGE201602005

Li, S. D., Li, X., Zhang, J., and Wang, Y. (2010). Study of Geological Origin Mechanism of Tangjiashan Landslide and Entire Stability of Landslide Dam. *Chin. J. Rock Mech. Eng.* 29 (S1), 2908–2915.

Liu, J. F., You, Y., and Chen, X. C. (2010). The Characteristics and Countermeasures of Dam-Breaking Debris Flow after Wenchuan Earthquake—A Case Study of the Tangfang Gully in Pingwu county,Sichuan Province. *J. Sichuan Univ. (Engineering Sci. Edition)* 42 (5), 68–75. doi:10.15961/j.jsuese.2010.05.007

Nian, T. k., Wu, H., Chen, G. Q., Zheng, D., and Li, D. (2018). Research Progress on Stability Evaluation Method and Disaster Chain Effect of Landslide Dam. *Chin. J. Rock Mech. Eng.* 37 (8), 1796–1812. doi:10.13722/j.cnki.jrme.2017.1655

Okura, Y., Kitahara, H., Kawanami, A., and Kurokawa, U. (2003). Topography and Volume Effects on Travel Distance of Surface Failure. *Eng. Geology*. 67, 243–254. doi:10.1016/s0013-7952(02)00183-7

Peng, S. Q., Xu, Q., Li, H. J., and Zheng, G. (2019). Grain Size Distribution Analysis of Landslide Deposits with Reliable Image Identification. *J. Eng. Geology*. 27 (6), 1290. doi:10.13544/j.cnki.jeg.2018-305

Qin, H. K., Zhang, H. Q., and Zhang, B. (2016). Formation Conditions of the Qipangou Multi Stage Dam-Breaking Debris Flow in Wenchuan Area after the Earthquake. *J. Eng. Geology*. 24 (s), 100–107. doi:10.13544/j.cnki.jeg.2016.s1.015

Savage, S. B., and Lun, C. K. K. (1988). Particle Size Segregation in Inclined Chute Flow of Dry Cohesionless Granular Solids. *J. Fluid Mech.* 189, 311–335. doi:10.1017/s002211208800103x

Shan, Y. B., Chen, S. S., and Zhong, Q. M. (2020). A Rapid Evaluation Method of Landslide Dam Stability[J]. *Chin. J. Rock Mech. Eng.* 39 (9), 1847–1859. doi:10.13722/j.cnki.jrme.2019.1240

Shi, Z. M., Guan, S. G., Peng, M., Zhang, L. M., Zhu, Y., and Cai, Q. P. (2015). Cascading Breaching of the Tangjiashan Landslide Dam and Two Smaller Downstream Landslide Dams. *Eng. Geology*. 193, 445–458. doi:10.1016/j.enggeo.2015.05.021

Shi, Z. M., Ma, X. L., Peng, M., and Zhang, L. (2014). Statistical Analysis and Efficient Dam Burst Modelling of Landslide Dams Based on a Large-Scale Database. *J. Rock Mech. Eng.* 33 (9), 1780–1790. doi:10.13722/j.cnki.jrme.2014.09.007

Shi, Z. M., Xiong, X., Peng, M., Zhang, L. M., Xiong, Y. F., Chen, H. X., et al. (2017). Risk Assessment and Mitigation for the Hongshiyan Landslide Dam Triggered by the 2014 Ludian Earthquake in Yunnan, China. *Landslides* 14 (1), 269–285. doi:10.1007/s10346-016-0699-1

Umbanhowar, P. B., Melo, F., and Swinney, H. L. (1998). Periodic,aperiodic,and Transient Patterns in Vibrated Granular Layers. *Physica A:Statistical Mech. its Appl.* 249 (1–4), 1–9. doi:10.1016/s0378-4371(97)00425-1

Wang, G. Q., Wang, Y. Q., Liu, L., and Wang, D. (2015). Reviewed on Barrier Dam and Simulation on Dam Breach. *Yellow River* 37 (09), 1–7. doi:10.3969/j.issn.1000-1379.2015.09.001

Wang, Y. F., Chen, Q. G., and Zhu, Q. (2012). Inverse Grading Analysis of deposit from Rock Avalanches Triggered by Wenchuan Earthquake. *Chin. J. Rock Mech. Eng.* 31 (6), 1089. doi:10.3969/j.issn.1000-6915.2012.06.002

Zhang, M., and Yin, Y. (2013). Dynamics, Mobility-Controlling Factors and Transport Mechanisms of Rapid Long-Runout Rock Avalanches in China. *Eng. Geology*. 167, 37–58. doi:10.1016/j.enggeo.2013.10.010

Zhang, S., Xie, X., Wei, F., Chernomorets, S., Petrakov, D., Pavlova, I., et al. (2015). A Seismically Triggered Landslide Dam in Honshiyan, Yunnan, China: from Emergency Management to Hydropower Potential. *Landslides* 12 (6), 1147–1157. doi:10.1007/s10346-015-0639-5

Zhao, G.-W., Jiang, Y.-J., Qiao, J.-P., Yang, Z.-J., and Ding, P.-P. (2019). Numerical and Experimental Study on the Formation Mode of a Landslide Dam and its Influence on Dam Breaching. *Bull. Eng. Geol. Environ.* 78, 2519–2533. doi:10.1007/s10064-018-1255-0

Zhao, T., Dai, F., and Xu, N.-w. (2017). Coupled DEM-CFD Investigation on the Formation of Landslide Dams in Narrow Rivers. *Landslides* 14, 189–201. doi:10.1007/s10346-015-0675-1

Zheng, G., Xu, Q., and Peng, S. Q. (2019). Mechanism Analysis of the Accumulation Characteristics of Rock Avalanche. *J. Eng. Geology*. 27 (4), 842–852. doi:10.13544/j.cnki.jeg.2018-241

Zheng, H., Shi, Z., Peng, M., Guan, S., Hanley, K. J., and Feng, S. (2022). Amplification Effect of Cascading Breach Discharge of Landslide Dams. *Landslides* 19, 573–587. doi:10.1007/s10346-021-01816-0

Zheng, H., Shi, Z., Yu, S., Fan, X., Hanley, K. J., and Feng, S. (2021). Erosion Mechanisms of Debris Flow on the Sediment Bed. *Water Resour. Res.* 57 (12), 1–19. doi:10.1029/2021WR030707

Zhou, G. G. D., Cui, P., Chen, H. Y., Zhu, X. H., Tang, J. B., and Sun, Q. C. (2013b). Experimental Study on Cascading Landslide Dam Failures by Upstream Flows. *Landslides* 10 (5), 633–643. doi:10.1007/s10346-012-0352-6

Zhou, G. G. D., and Ng, C. W. W. (2010). Numerical Investigation of Reverse Segregation in Debris Flows by DEM. *Granular Matter* 12 (5), 507–516. doi:10.1007/s10035-010-0209-4

Zhou, J.-w., Cui, P., and Fang, H. (2013a). Dynamic Process Analysis for the Formation of Yangjiagou Landslide-Dammed lake Triggered by the Wenchuan Earthquake, China. *Landslides* 10 (3), 331–342. doi:10.1007/s10346-013-0387-3

Zhou, Y., Shi, Z., Zhang, Q., Jang, B., and Wu, C. (2019b). Damming Process and Characteristics of Landslide-Debris Avalanches. *Soil Dyn. Earthquake Eng.* 121, 252–261. doi:10.1016/j.soildyn.2019.03.014

Zhou, Y., Shi, Z., Zhang, Q., Liu, W., Peng, M., and Wu, C. (2019a). 3D DEM investigation on the morphology and structure of landslide dams formed by dry granular flows. *Engineering Geology* 258 (14), 105151. doi:10.1016/j.enggeo.2019.105151

Conflict of Interest: The authors declare that the research was conducted in the absence of any commercial or financial relationships that could be construed as a potential conflict of interest.

Publisher's Note: All claims expressed in this article are solely those of the authors and do not necessarily represent those of their affiliated organizations, or those of the publisher, the editors, and the reviewers. Any product that may be evaluated in this article, or claim that may be made by its manufacturer, is not guaranteed or endorsed by the publisher.